Variability of the Great-Whirl from Observations and Models

Achim Wirth, J. Willebrand, F. Schott

Variability of the Great Whirl from observations and models

A. Wirth*, J. Willebrand, F. Schott

Institut für Meereskunde, Universität Kiel, Duesternbrooker Weg 20, 24105 Kiel, Germany

Observations from cruises in the Arabian Sea and data from satellites are interpreted using different realizations of a multi-level primitive equation model and an eddy-permitting reduced-gravity shallow water model of the Indian Ocean. The focus is on the interannual circulation variability of the Arabian Sea, and especially of the meridional location of the Great Whirl (GW). The results suggest that the variability in the western Arabian Sea is not only due to the interannual variability in the wind field, but that a substantial part is caused by the chaotic nature of the ocean dynamics. Decreasing the friction coefficient from 1000 to 500 $m^2\ s^{-1}$ in a $\frac{1}{9}^\circ$ numerical reduced-gravity model, the variance of the GW location increases dramatically, and the mean position moves southward by one degree. In the eddy-permitting experiments analyzed, both mechanisms appear to determine the GW location at the onset of the GW dynamics in late summer.

1. Introduction

During the German Meteor and Sonne cruises in 1993, 1995 and 1996 and related moored observations in the western Arabian Sea, considerable year-to-year differences in the ocean circulation were found (e.g., Schott and McCreary, 2001). The cruises, which took place in late summer, investigated the dynamics in the western Arabian Sea. In that time of year, strong south westerly Monsoon winds lead to a strong Somali current flowing northward along the coast of Africa. The most conspicuous phenomenon in this area is the Great Whirl (GW), a large anti-cyclonic eddy that develops every year after the onset of the summer monsoon (Schott and Quadfasel, 1982). The GW not only causes substantial upwelling along the coast of Africa but also transports and mixes the cold upwelled water eastward into the interior Arabian Sea (Schott, 1983). The dynamics of the GW is thus important for the region's sea-surface temperature and for the meridional heat transport. The signature of the GW is also clearly visible when considering biological production in the Arabian Sea (McCreary et al., 1996). It is thus of great importance to consider variability, especially the interannual variability of the GW system.

The interannual variability of the ocean circulation in principle can have two sources, an external and an internal one. Year-to-year changes in atmospheric forcing, which in the Arabian Sea mainly result from variability of the wind field, obviously lead to externally-forced variability in ocean dynamics. Internal oceanic variability can

*Corresponding author. Fax: +49-0431-597-3882.
E-mail address: awirth@ifm.uni-kiel.de (A. Wirth).

result from the instability of ocean currents due to the nonlinearity of the equations governing the dynamics of the ocean.

The distinction between internal and external variability is important for the interpretation of the observed data, and for any comparison of model results with observations. If the internal variability is negligible, a one-to-one comparison between model results of the Indian Ocean circulation and observations should be feasible, provided that the ocean model and wind forcing are sufficiently accurate. On the other hand, if the internal variability is not negligible, a direct model–data comparison even with a perfect model is meaningless except in the context of data assimilation, and one can only compare statistical parameters such as mean values, variances or correlations of quantities important to the ocean circulation.

When interannual variability in the Indian Ocean has been considered in previous modeling studies, the emphasis has been focused almost entirely on external variability. Internal variability has been argued to play no substantial role since the early work by Luther and O'Brien (1989) and usually is neglected altogether (e.g., Anderson and Carrington, 1993; Luther, 1999). Obviously, this neglect is meaningful only when using models with relatively coarse resolution and/or rather high values of the friction parameters where the internal variability is small or nonexistent. When models of higher resolution and smaller friction values are employed, the chaotic nature of the underlying ocean dynamics is revealed, showing up not only at small scales but potentially also at large scales.

Based on the results of eddy-permitting and eddy-resolving models, we argue here that in the western Arabian Sea the internal variability is indeed substantial. Specifically, our purpose is to quantify and compare external and internal variability in the western Arabian Sea.

2. Observations

The observations used are from recent WOCE measurements and from TOPEX/Poseidon satellite altimetry. The in situ observations consist of shipboard hydrography and acoustic doppler current profiling (ADCP) sections across the Northern Somali Current and Great Whirl during the summer monsoons of 1993 (Fischer et al., 1996) and 1995 (Schott et al., 1997), and also of moored current measurements. The mooring records cover a period of 18 months in 1995–96, including both summer monsoons, with stations deployed along a near-meridional line running southward from the island of Socotra at approximately 54°E.

As described above, the "Great Whirl" develops with the monsoon onset in June in the 4–10°N latitude range, with a cold wedge at 10–12°N, the latitude where it turns offshore (Fig. 1). The cross-equatorial flow continues during this time, carrying a transport of about 20 Sv in the upper 500 m. It leaves the coast south of 4°N, where it partially turns eastward, also with an upwelling wedge at its northern shoulder, and partially flows back across the equator to form the "Southern Gyre" (Fig. 1). Water-mass signatures of both gyres indicate little exchange between the Great Whirl and the Southern Gyre at this time, at least in the upper layers. Thus, water that crosses the equator does not continue to flow up the Somali coast, but rather bends eastward at low latitudes to flow into the interior of the Arabian Sea.

In the late phase of the summer monsoon, the Great Whirl has become an almost-closed circulation cell (Fig. 1) with very little exchange between its offshore recirculation branch and the interior Arabian Sea, as is apparent from the differences in surface salinities between the GW and the region to the east of it (Fig. 1). To the north, another anticyclonic feature, the Socotra Gyre (Fig. 1), develops in some seasons. GW transports in this late summer monsoon phase can exceed 70 Sv (Fischer et al., 1996; Schott et al., 1997), and strong upwelling exists where the flow turns offshore. During particularly strong upwelling episodes, upwelled waters can be colder than 17°C (Swallow and Bruce, 1966), but typical upwelling temperatures are in the 19–23°C range.

When the Southwest Monsoon dies down, the cross-equatorial Somali Current turns offshore again at 3°N, while the Great Whirl continues to spin in its original position. The Great Whirl is

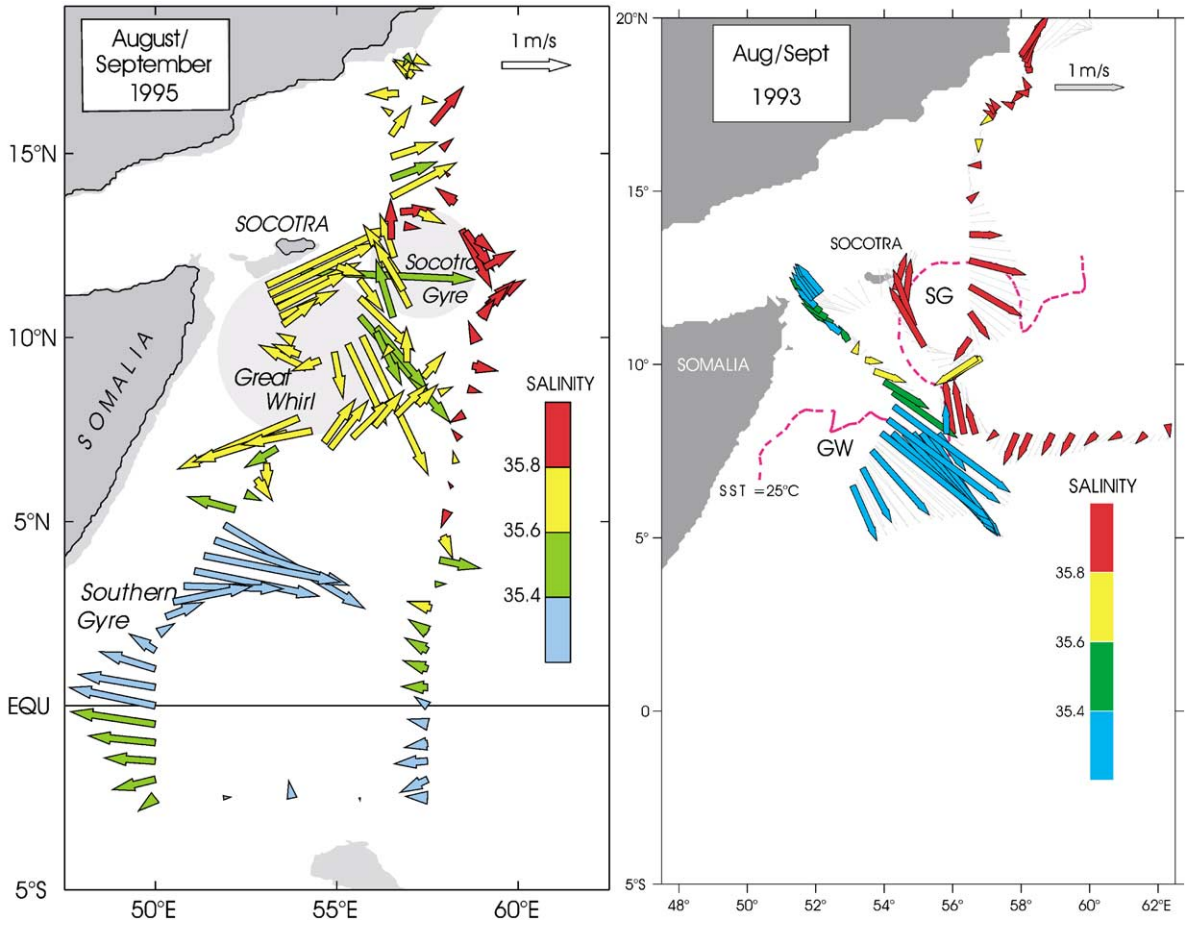

Fig. 1. Somali Current flow patterns during the late summer monsoon phases of (a) 1993 and (b) 1995. Marked are the Southern Gyre, Great Whirl and Socotra Gyre. Near-surface salinities (color-coded on the current vectors) indicate that lower-salinity waters originating from the southwestern and upwelling regions recirculate in the Great Whirl. Note that the GW in 1995 was located much more northerly, against the banks of southern Socotra, than in 1993 (after Fischer et al., 1996 and Schott et al., 1997).

even discernible underneath the developing Northeast Monsoon circulation well toward the end of the year (Bruce et al., 1981).

Significant interannual differences in the system of cold upwelling wedges off Somalia and their movements during the course of the Southwest Monsoon have already been reported (Evans and Brown, 1981; Schott, 1983). Recently, based on the WOCE moored and shipboard observations during 1993–96, new analyses as to the location and intensity of the Great Whirl have been made (Fig. 2). In 1993, the northern boundary of the Great Whirl was located about 200 km south of the banks of Socotra (Fischer et al., 1996). In 1995, it was banked right against the slope south of Socotra (Schott et al., 1997), and it was well developed as one large organized circulation cell until mid-October. In 1996, it was again located much more to the south, similar to the 1993 situation, the gyre transports were weaker than in 1995, and the Great Whirl was already becoming disorganized in August (Fig. 2).

For an analysis of the changes in the GW position, we have used altimetry data from the CLS Space Oceanography Division giving the sea-surface anomaly every 10 days. These data can be

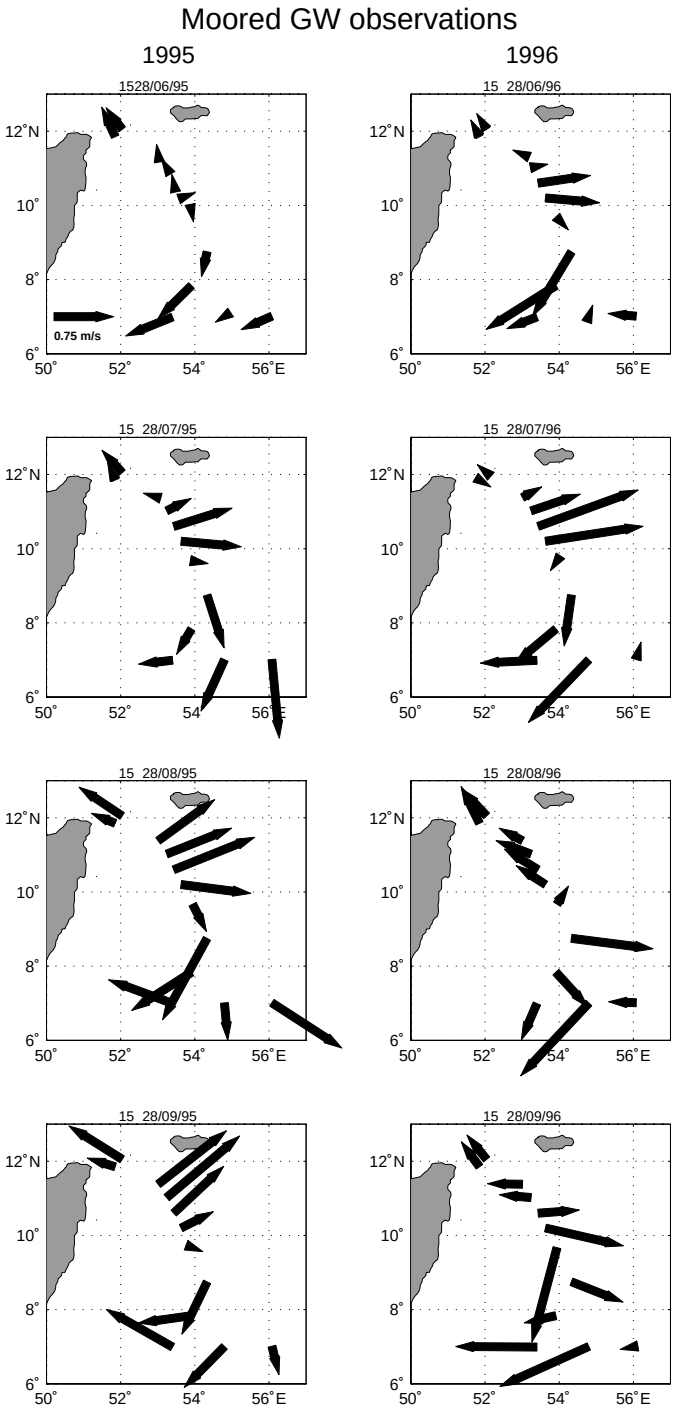

Fig. 2. Time series of near-surface current vector plots from the Great Whirl and Socotra Passage region (15 day means) for June–September (a) 1995, (b) 1996. Note the differences in GW intensities of both years and that the 1996 GW collapsed much earlier (from Schott and McCreary, 2001).

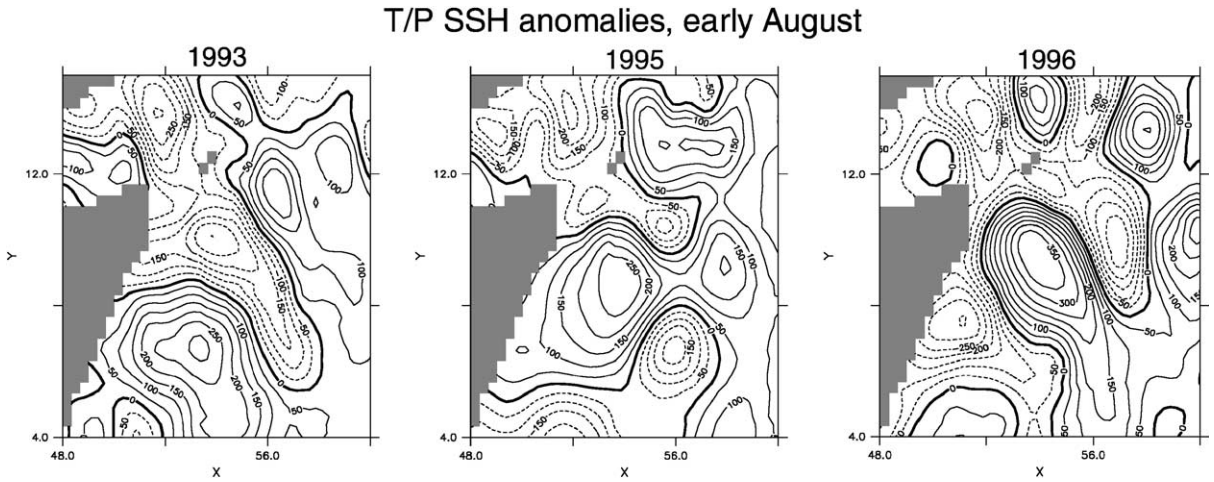

Fig. 3. Altimetric sea-surface height anomalies (in mm) in early August for the years 1993, 1995, and 1996.

downloaded from: ftp.cls.fr/pub/oceano/AVISO/MSLA; details can be found in Le Traon et al. (1998) and Le Traon and Ogor (1998). During the months of July and August, the GW could be detected by a sea-surface height anomaly (SSHA) which is maximum in the regions between 6°N and 12°N and between 50°E and 56°E. As seen from Fig. 3, the location of the GW maximum is usually located within this area. Each SSHA map was also inspected visually. At later times of the GW evolution, that is, in September and October, the identification of the GW was ambiguous as it sometimes splits up, was dominated by a stronger Socotra gyre (see Fig. 1), or had left the region described above. We therefore have restricted our analysis of the GW position to the months of July and August.

3. The models

When analyzing ocean dynamics with the use of complex numerical models, a balance between realism, comprehension and feasibility has to be found. To this end, it is often useful to employ a hierarchy of models of different complexities, to untangle the ocean dynamics. We therefore have employed two different classes of models, namely a fully thermodynamic multi-level primitive equation (PE) model and a reduced-gravity (RG) model.

The rationale for this choice is as follows. The PE model permits a fairly realistic simulation of the circulation, however, at a high computational expense so that only very few integrations were possible. The RG model is much simpler and lags many important processes that are represented in the PE model such as, for example, baroclinic instability, the influence of salinity and realistic topography. This has important effects on the solution, as mentioned in Section 5. However, a large number of experiments with a higher horizontal resolution are possible with the RG model that can help to evaluate the chaotic nature of the ocean circulation.

Each model has been used in two configurations, with high and low friction, in order to estimate the sensitivity of the solution to the dissipation parametrization.

3.1. Primitive equation model

The PE model was constructed on the basis of the MOM2.1 code with a $1/3^\circ \times 1/3^\circ$ resolution and 35 vertical levels, 10 of which are in the upper 110 m. The model extends from 30°S to 26°N and from 30°E to 110°E, with open boundaries at 30°S and at 115°E (Indonesian Throughflow) that are

treated following Stevens (1990). Values for the transport streamfunction and the tracers at inflow points were taken from the model of Semtner and Chervin (1992). The vertical mixing of tracers and momentum depends on the Richardson number, following Pacanowski and Philander (1981). Surface salinity is relaxed to the monthly mean values given by Levitus and Boyer (1994). A description of the model is given by Rix (1998), who also discusses some general aspects of the model's circulation.

In its standard version, the model has biharmonic horizontal diffusion and friction, with a coefficient of 3×10^{11} m^4 s^{-1}, which is chosen as small as possible to be compatible with numerical requirements. Alternatively, a version with horizontal Laplacian diffusion was employed with a coefficient of 1×10^3 m^2 s^{-1}. While biharmonic mixing is physically somewhat less justified than Fickian diffusion, it has the advantage that it acts only at the smallest resolved scales, and at the mesoscale is, therefore, less dissipative than Laplacian diffusion. For example, for a length scale of 100 km, the diffusive time scale in the Laplacian version is 100 days, compared to 3000 days in the biharmonic version.

3.2. Reduced gravity model

In the construction of the RG model, we closely followed the model proposed by McCreary and Kundu (1989). The model domain extends from 10°S to 20°N and from 38°E to 98°E with closed boundaries in the south and east (no Indonesian Throughflow), and has a horizontal resolution of $\frac{1}{9}^\circ \times \frac{1}{9}^\circ$. The model consists of a dynamic layer of average thickness 200 m, including a 50 m thick mixed layer. The dynamic layer and the mixed layer that both have a horizontally varying temperature lie above a deep inert layer with a temperature of 16°C. The effects of salinity are neglected. When the dynamic layer becomes shallower than the mixed layer, deep water is entrained into the mixed layer and the thickness of the dynamic layer is set to the mixed-layer depth. This process parameterizes the upwelling that usually occurs at one or two coastal wedges along the coast of Somalia (see Schott, 1983).

In the RG model, the lateral viscosity coefficient equals the diffusivity coefficient and will henceforth be referred to as the "friction" coefficient. It has a standard value of 5×10^2 m^2 s^{-1}, which is again chosen as small as possible to keep the numerical noise at an insignificant level. For comparison, a high-friction version with twice that value is also used.

4. The experiments

4.1. Primitive equation solutions

Two experiments with the PE model spanning the period from 1970 to 1996 were performed (Table 1). Experiment PE-hi used Laplacian friction, while experiment PE-lo used the

Table 1
Overview of the numerical experiments performed

Exp.	Forcing	Friction (10^3 m^2/s)	Horiz. res. (deg)	Ensemble size
PE-hi	FSU70-96	1	1/3	1
PE-lo	FSU70-96	(*biharm.*[a]) 3×10^{11} m^4 s^{-1}	1/3	1
RG-hi93	FSU93	1	1/9	10
RG-lo93	FSU93	0.5	1/9	10
RG-hi95	FSU95	1	1/9	10
RG-lo95	FSU95	0.5	1/9	10
RG-hi96	FSU96	1	1/9	10
RG-lo96	FSU96	0.5	1/9	10
RG-200	Climatology	0.7	1/9	200

[a] Viscosity = 3 and diffusivity = 5×10^{11} m^4 s^{-1}.

biharmonic formulation. Both the experiments started from the same 30-year-long spin-up using climatological forcing (no interannual variability). The wind forcing has been derived from the observed monthly mean pseudostress data of Florida State University (FSU) for the years 1970–1996. For the surface heat flux, we have used the formulation by Barnier et al. (1995), which can be interpreted as a relaxation of the model surface temperature towards an equivalent surface temperature determined from a climatology based on the data from ECMWF.

A snapshot (August 1) of the depth-integrated transport in both model versions in the western Arabian Sea is shown in Fig. 4 (left panel). Both models display a GW structure in this variable with roughly the same overall magnitude. As expected, the biharmonic version (Exp. PE-low) shows a narrower boundary current and more intense flow around the GW, and is accompanied by a cyclonic eddy that is barely seen in Exp. PE-hi.

4.2. Reduced-gravity solutions

In the experiments with the RG model, it has been attempted to distinguish between the external variability forced by the wind and the internal variability generated by ocean processes. For this reason, integrations with the RG model using FSU wind forcing of each of the perpetual years 1993, 1995 and 1996 have been performed, both for high and low values of the friction coefficient (Table 1). Each integration consisted of a 5-year spin-up followed by 10 years, which were used for the analysis. By considering large-scale quantities like the meridional heat transport and the GW location, it was checked that the model reached a statistically stationary state after only about three years.

By forcing the model repeatedly with a perpetually repeated annual-cycle wind pattern, we implicitly assume that the model dynamics has an effective memory time of less than 1 year. This has been checked by performing one integration over 200 years (Exp. RG-200) with perpetual winds. In this experiment, the spectrum of annual averaged variables such as the meridional heat transport was indistinguishable from a white spectrum, suggesting that the memory of the model is indeed smaller than 1 year. This rather short time scale is in agreement with the equatorial and low latitude dynamics of the RG model. Equatorial waves in the Indian Ocean and planetary waves in the Arabian Sea take considerably less than 1 year to cross the corresponding basin (e.g., Philander, 1990). It is therefore, justified to consider the result from two consecutive years in the RG model as approximately statistically independent, so that each integration effectively yields an ensemble of 10 independent realizations.

Fig. 4 (right panel) shows the mean layer thickness in Exps. RG-lo95 and RG-hi95. In order to suppress the internal variability, an average of 10 subsequent realizations was taken. Note that in the low-friction experiments, the average GW intensity is higher and the meridional location of the GW position is more southward by about 1° for all wind forcings considered compared to the high-friction cases. This is most probably caused by the earlier occurrence of instability in the low-friction case.

In the RG model, the center of the GW was defined as the point with the maximum thickness of the dynamic layer in the Arabian sea. Likewise, in the PE model, the center of the GW is defined as the location where the 20°C thermocline is the deepest. The meridional location of the GW center obtained in this way from July 1 to September 1 in the different experiments is given in Table 2. As discussed above, at later times during the year the GW location is no longer meaningful due to turbulent eddies.

5. Wind-induced (external) variability

In order to investigate the extent to which the observed variability in the GW region can be attributed to the wind, we first consider the wind stress curl for August 1 of the years 1993, 1995 and 1996. The flat-bottom Sverdrup transport stream function has a maximum in the GW area for the years 1993 and 1996, while the maximum is more southward in 1995. As seen from Table 2, in both the altimeter observations and the numerical

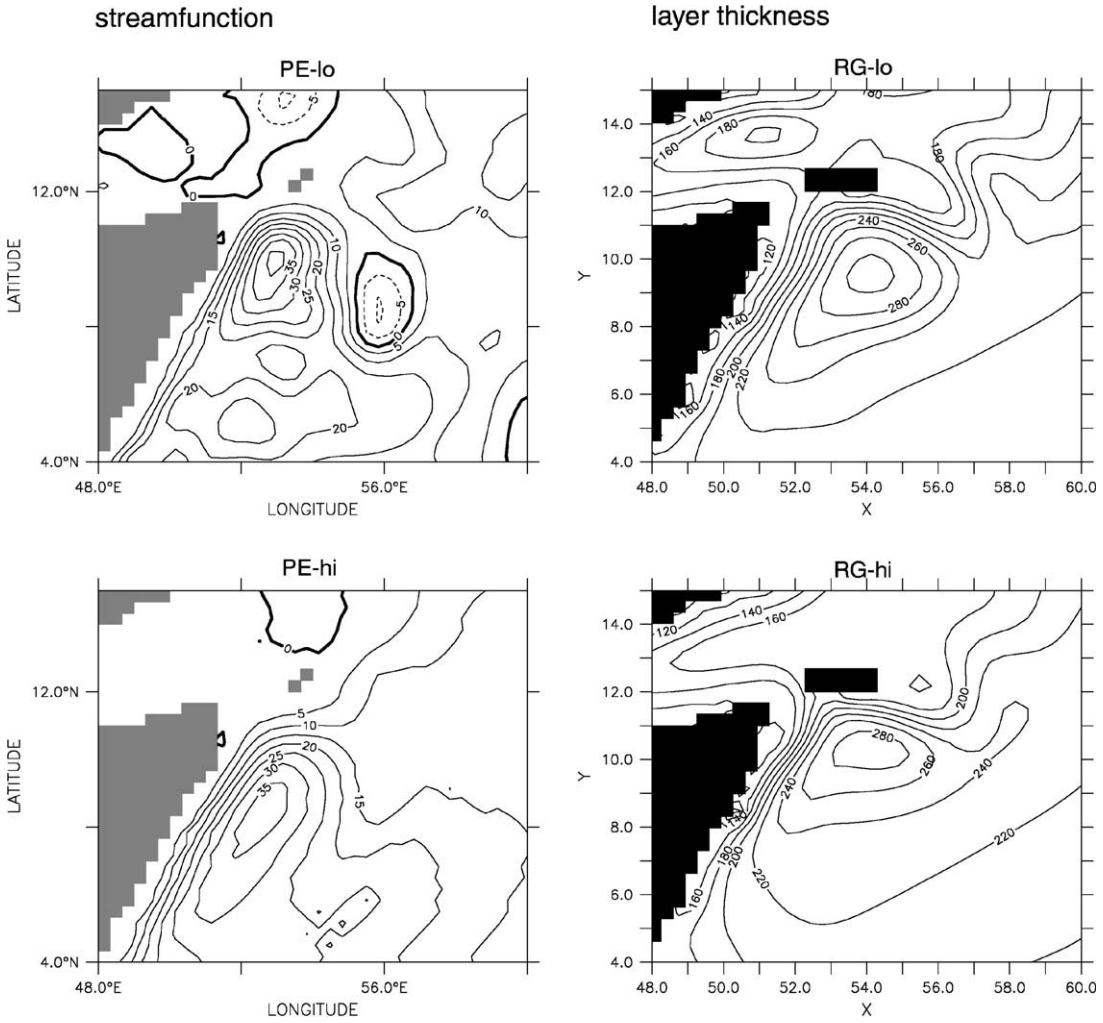

Fig. 4. Circulation patterns in 4 different experiments. Left panels: Snapshots of the depth integrated transport stream function from experiments PE-lo (top) and PE-hi (bottom), taken on August 1, 1995. Contour interval 5 Sv. Right panels: Mean layer thickness of the reduced-gravity model (averaged over 10 subsequent August 1) for experiments RG-lo95 (top) and RG-hi95 (bottom). Contour interval 20 m.

simulations, the center of the GW is more northward in the year 1995 compared to 1993, in contrast to the results obtained from the flat-bottom Sverdrup balance (see also Table 2). Hence, the linear flat-bottom Sverdrup balance is obviously not the key to determine the position of the GW, as was already discussed by Cox (1979).

For Exp. PE-lo, which can be considered to be more realistic than PE-hi, the near-surface temperature and velocity for the summers 1993 and 1995 (Fig. 5) can be compared directly with the observations in Fig. 1. As in the observations, the GW center in 1993 is 200 km more southward than in 1995 (cf., Table 2). Fig. 6 shows the difference between the years 1995 and 1993 for the altimetric observations and the two PE models. Despite the different nature of the variables (SSH for the observations, barotropic transport stream function for the models) the change from 1993 to 1995 is at least qualitatively reproduced in PE-lo,

Table 2
Meridional GW location on August 1 of the years 1993, 1995, and 1996 in observations and models[a]

Obs./model	GW Pos 93	GW Pos 95	GW Pos 96
Altimetry	6.6	8.4	9.2
Sverdrup trans.	10.0	8.7	9.0
RG—high	9.8	10.1	9.8
RG—low	8.7 ± 0.5	9.5 ± 0.3	9.0 ± 0.3
PE—high	8.0	9.0	8.1
PE—low	7.1	9.1	7.1

[a] Note that for the altimetry, the location of the *anomaly* maximum is given so that only the year-to-year differences can be compared.

and to a lesser extent also in PE-hi where that difference is considerably smaller.

As also seen from Fig. 6, however, the changes from 1993 to 1996 are not well reproduced in either of the PE models. In both experiments, the GW in 1996 has only about half the transport compared to 1993 and 1995 (not shown). The observed sea-surface height anomalies on August 1 of 1996 however, are, comparable in magnitude to the years 1993 and 1995 (cf. Fig. 3). A closer analysis for the year 1996 reveals that observations and numerical simulations still agree to some extent in July, but the GW starts to disappear early in 1996. On August 1, the GW disappearance in the two PE experiments has already proceeded, while in the observations it happens only about 10 days later.

On average, the RG models agree with the observations in giving a more southward position of the GW in 1993 compared to 1995. This is true for both high- and low-friction experiments. In the low-friction runs, individual realizations of Exps. RG-lo93 and RG-lo95 can, however, be found where this is not the case. Furthermore, in all realizations of Exps. RG-hi96 and RG-lo96, the RG model fails to reproduce the early break down of the GW that occurred in 1996. This is in contrast to the PE model, which shows this breakdown in both experiments, although not always at the same time as in the observations. A likely explanation could be that the dynamics of the single-layer RG model does not allow for baroclinic instability which plays an important role in the breakup of the GW according to Jensen (1993). Another possible reason might be the influence of the southern Indian Ocean, which is only partly (down to 10°S) included in the RG model.

6. Internal variability

The experiments with the RG model were conducted to determine the internally generated contribution to the interannual variability of the circulation in the Arabian Sea. Fig. 7 shows the layer thickness anomaly (relative to ensemble mean) in early August for three consecutive years of Exp. RG-lo95. Although there is no interannual variability in the forcing fields, substantial changes in the strength, shape and location of the circulation anomalies occur in the western Arabian Sea. This year-to-year variability is to be expected because, due to the chaotic dynamics of the model, every year the integration starts with different initial conditions which amplify in areas where the nonlinearity in the governing equations plays a substantial role. In the western-half of the Arabian Sea, the internal variability is elevated during the entire year. In the eastern part, the dynamics in the RG model is, however, more linear and the internal variability plays no substantial role.

Fig. 8 gives a comparison between externally and internally forced variability for the thickness anomaly. The upper figure shows the rms difference between the three mean values of the ensembles RG-lo93, RG-lo95 and RG-lo96 which result from the different wind forcing in the 3 years, and thus is a measure for the external variability. Maximum rms values reach more than 30 m in the western Arabian Sea. The lower part of Fig. 8 is the average rms within the three ensembles, and hence is a measure for the internal variability. It follows from Fig. 8 that the overall magnitude of the external and the internal variability is very similar in the GW region.

It is remarkable that increasing the friction coefficient by a factor of 2 is sufficient to virtually eliminate the internal variability. As seen in Fig. 9, the internally caused layer thickness variability is less than 5 m except in a small part of the area around the southern gyre and the GW, whereas

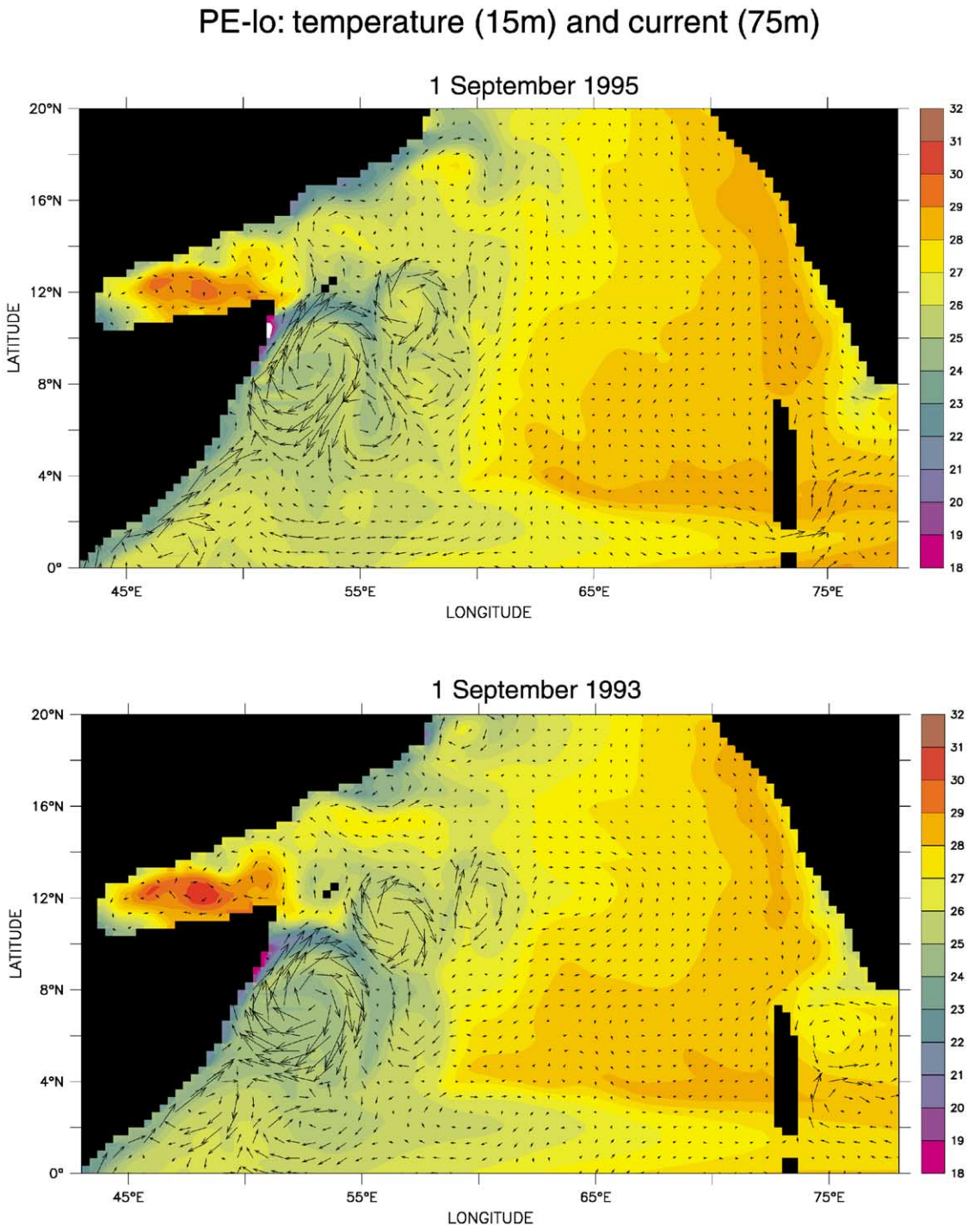

Fig. 5. Temperature at 15 m depth and velocity at 75 m depth on September 1 of 1995 (upper) and 1993 (lower) in the PE model (exp. PE-lo).

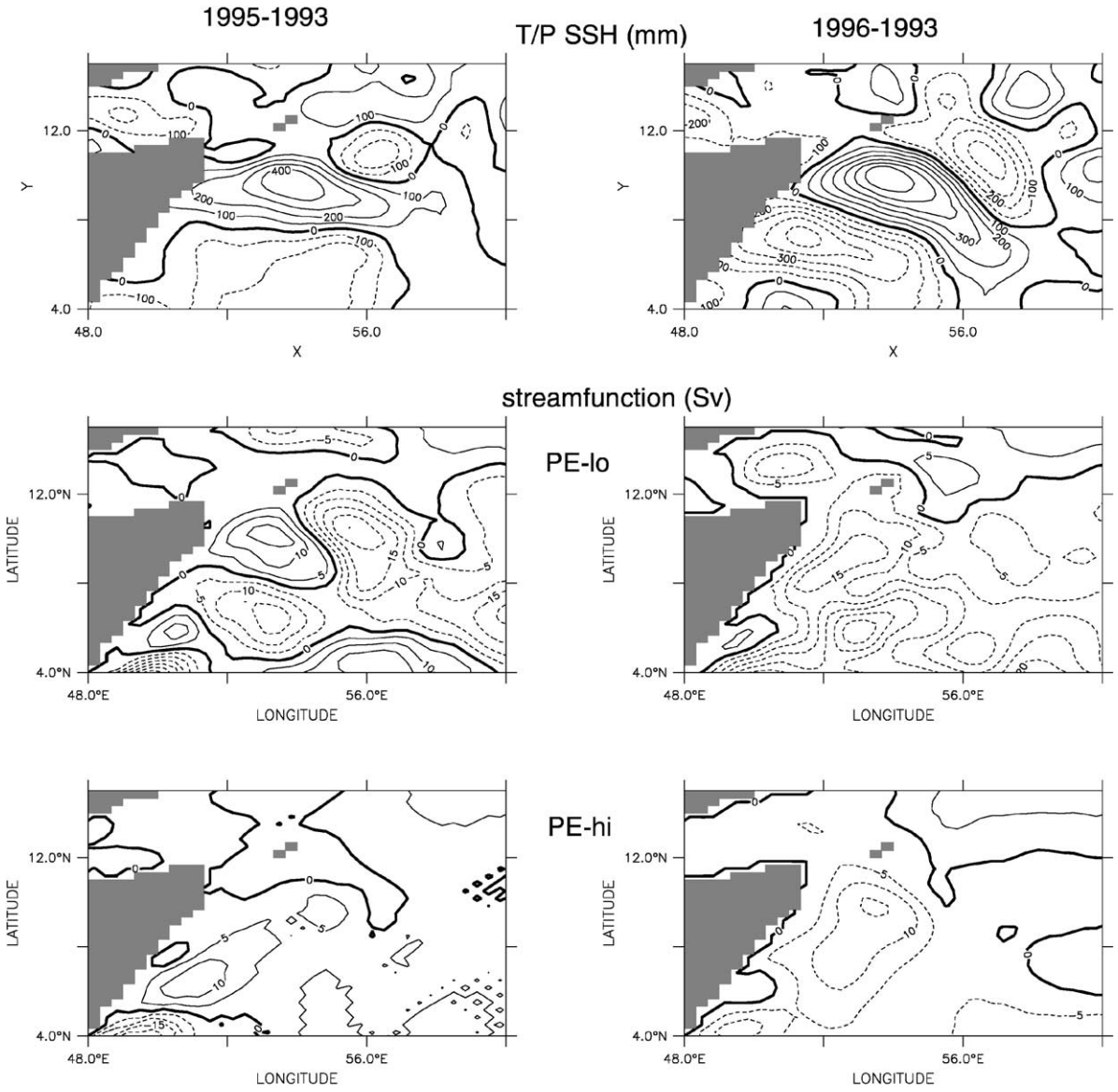

Fig. 6. Interannual variability of the GW on August 1. Left panels show values for 1995 minus 1993, right panels 1996 minus 1993. Top panels gives SSH from Topex/Poseidon (in mm), middle and bottom panels show depth integrated transport stream function from exp. PE-lo (middle) and PE-hi (bottom), both in Sv.

the externally forced interannual variability is only moderately reduced (maximum near 20 m layer thickness). In the RG-hi models, the GW therefore shows no substantial internal variability, a result that is consistent with Luther and O'Brien (1989).

Fig. 10 shows the GW meridional location vs. intensity as measured by the mean maximum layer thickness for the integrations with the RG model. In the high viscosity experiments, the wind forcing leaves a clear imprint in the GW intensity and to a lesser extent also in the GW location, with 1993

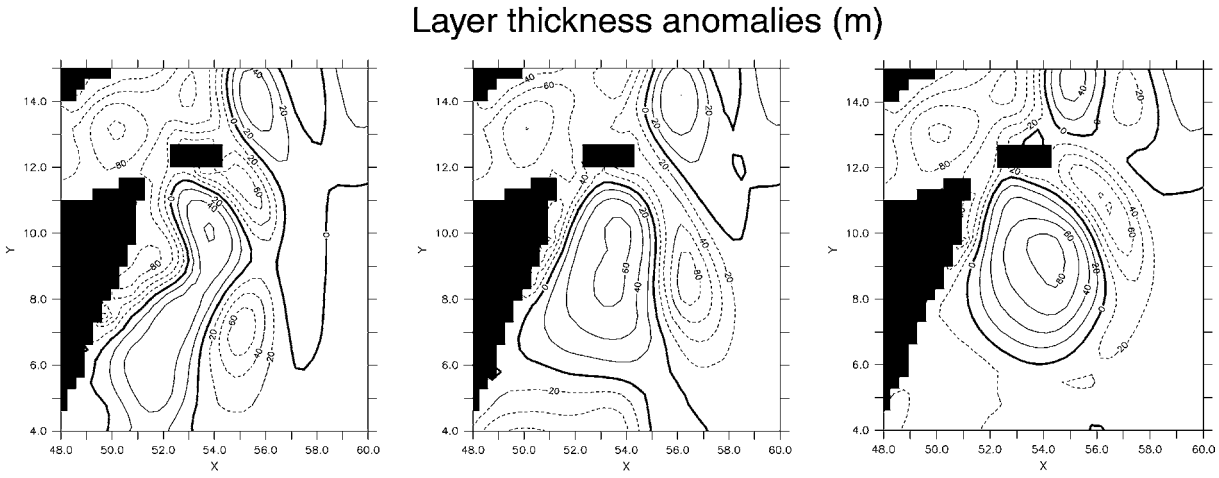

Fig. 7. Layer thickness anomalies (in m) relative to 10-year mean of all months at 3 consecutive August 1 in the low-friction experiment RG-lo95.

being the strongest and 1996 the weakest, and very little internal variations among the different ensemble members. In the low-friction experiments, the wind influence remains clearly visible but is superposed by a considerable scatter among the different ensemble members, with on average stronger GW realizations located more southward. Since the different members of each ensemble are subject to identical forcing, this scatter, which amounts to differences in meridional location by more than 100 km and in maximum layer thickness by more than 30 m, can only have internal causes.

The differences in GW location between the three ensembles also follow from Table 2 where the meridional GW positions for the 3 years, and the respective standard deviations are given. Furthermore, from the observed SSH anomalies it follows that the differences in location of the altimetric anomalies are larger than the differences in GW location between any of the models, suggesting that in the ocean the large-scale variability is even higher than in the models considered here. Indeed, experiments with the RG model with even lower friction values (not shown) indicate that the variability of large-scale features increases even further.

Within each of the three sets of Exps. RG-lo93, RG-lo95 and RG-lo96, we also have calculated the correlation of GW location and strength between July 1 and August 1 and between July 1 and September 1. The results are similar for the GW location and GW strength, showing significant correlations between July 1 and August 1 ranging from 0.45 to 0.72. The correlations between July 1 and September 1 are however insignificant. This suggests that the knowledge of the GW position and strength on July 1 does not improve a prediction of the same variables on September 1. This alludes to a correlation time for the GW location of roughly one month.

7. Discussion

The western Arabian Sea, like the western parts of all the ocean basins, is dominated by strong boundary currents that lead to instabilities, especially in low latitudes. In these areas, nonlinearity is higher than in the interior and eastern parts of the basins, leading to a higher ratio of internal vs. external variability. At the beginning of this work, it was intended to describe and classify the behavior of the GW during its life cycle in comparison with observations. We found, however, that this was not possible in eddy-permitting models. After a more or less annually recurrent birth period of the GW in July and

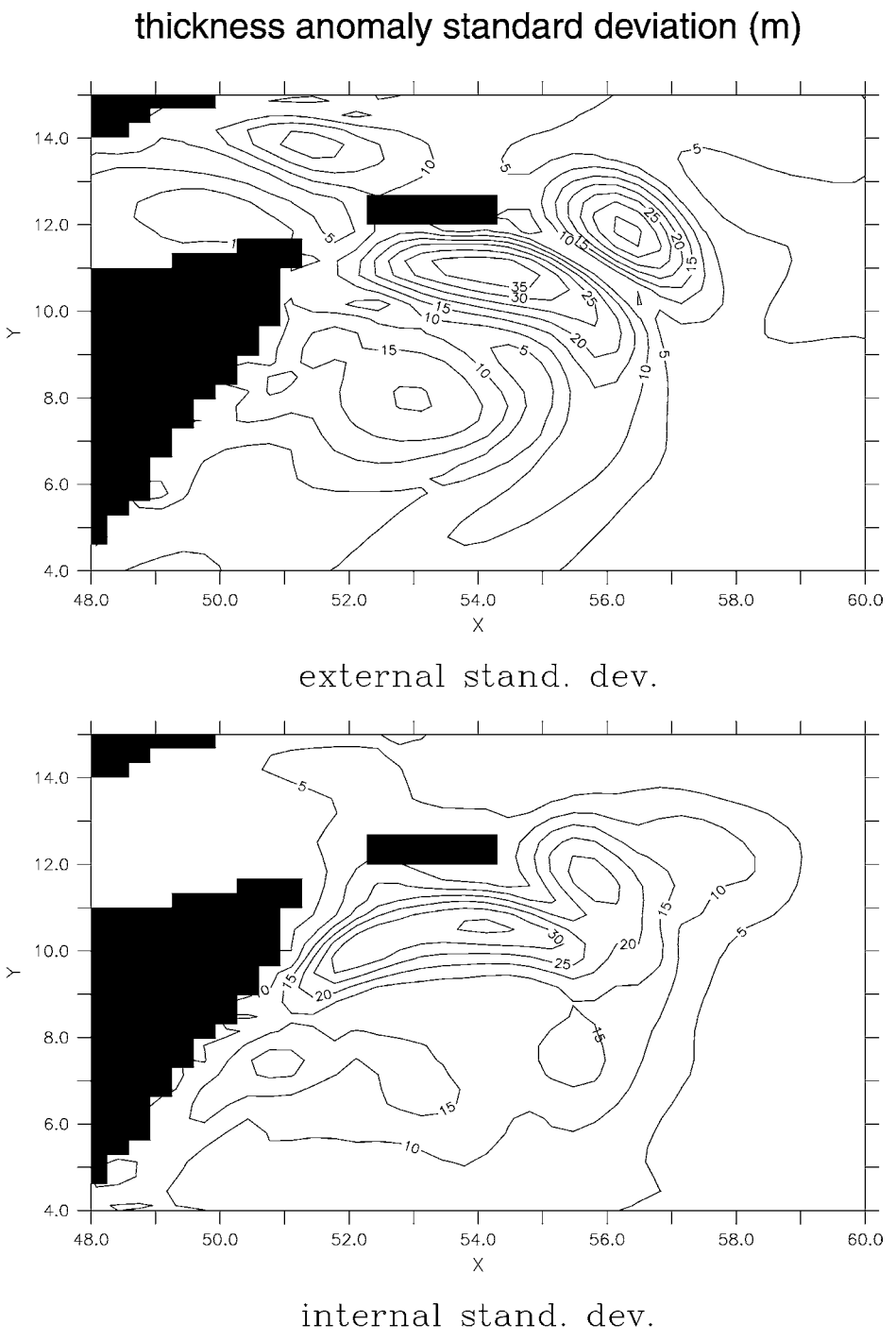

Fig. 8. Standard deviation due to external (upper) and internal (lower) variability for the low-viscosity exps. RG-lo (contour interval is 5 m). The standard deviation due to the external part is calculated using the variance of the means over 10 realizations for each of the years 1993, 1995 and 1996. The standard deviation of the internal part is calculated using the average variance for the years 1993, 1995 and 1996.

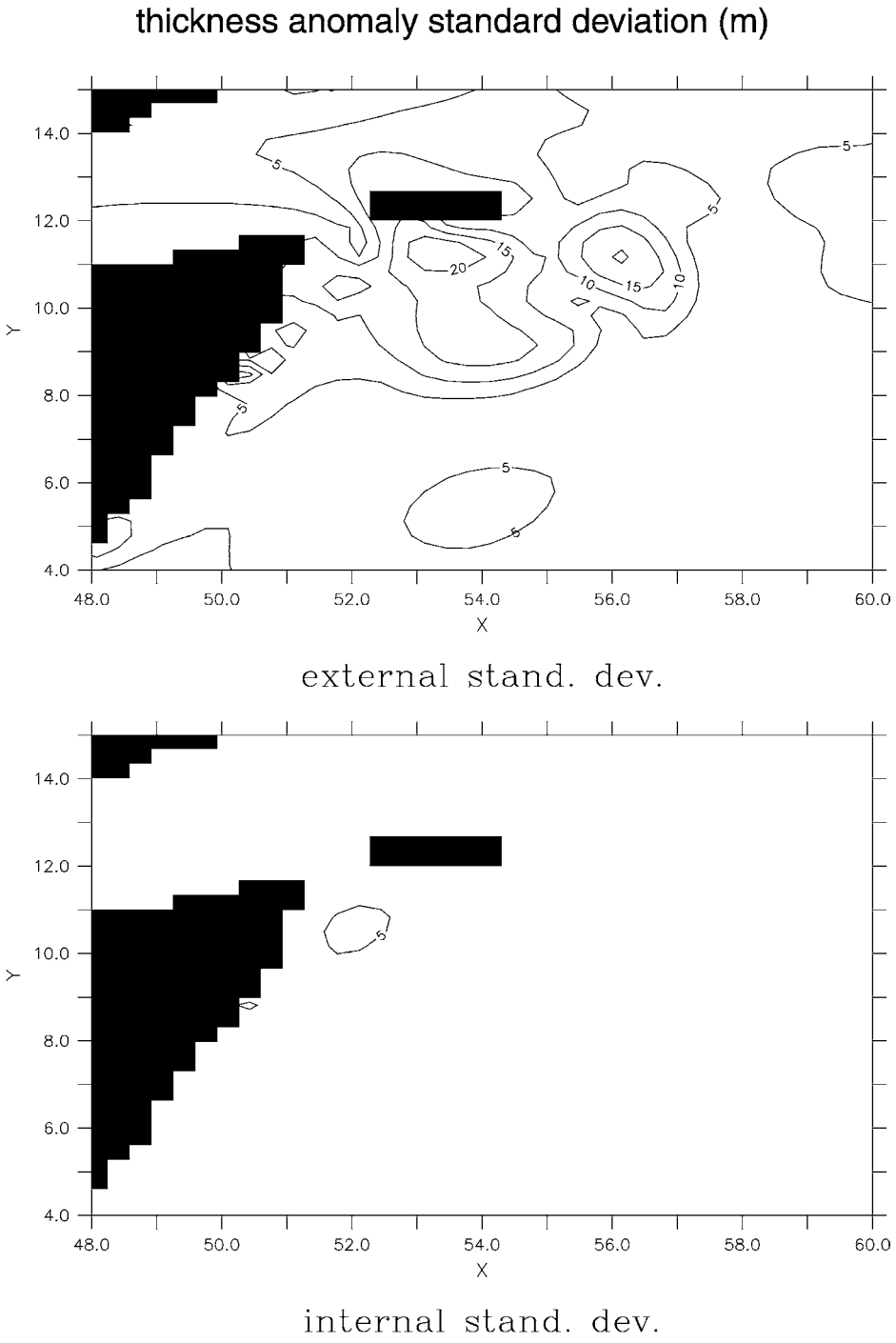

Fig. 9. As Fig. 8, but for the high-viscosity experiments RG-hi.

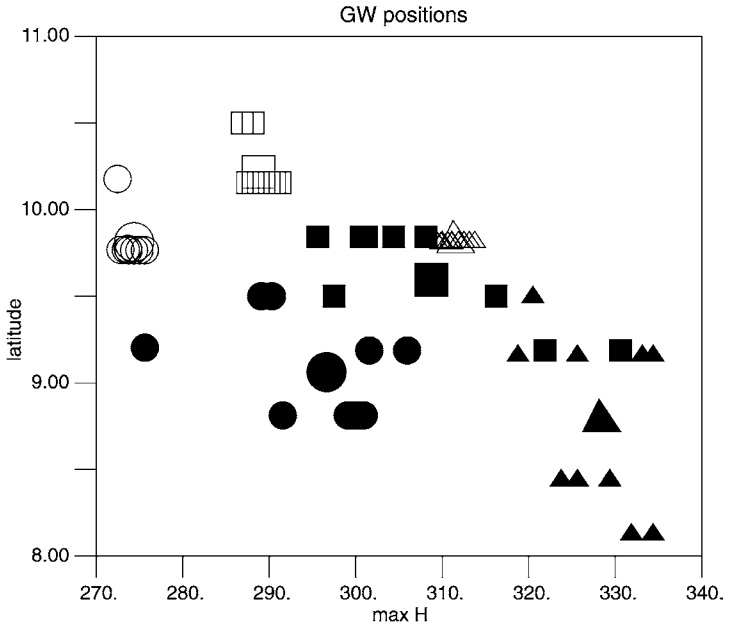

Fig. 10. Mean layer thickness vs. meridional position of the GW in the different experiments with the RG model. Triangles, squares and circles correspond to exps. with forcings of the years 1993, 1995 and 1996, respectively; solid and open symbols are for low and high-friction experiments, respectively; large symbols represent the mean values.

August, the circulation in the western Arabian Sea is strongly influenced by turbulent (mostly anticyclonic) eddies. Consequently, from September on the GW is characterized by chaotic dynamics rather than a regular life cycle.

We have demonstrated that the year-to-year variability of ocean currents in the western Arabian Sea is not only influenced by variability in the wind forcing but is substantially influenced by internally generated variability. This latter variability has a white spectrum on interannual time scales, and a prediction of the internally caused variability seems impossible on time scales longer than a month.

A critical parameter in the RG model is dissipation values that have been chosen here for reasons of numerical stability and smoothness. This choice, while common, is not based on physical considerations, and an uncomfortable conclusion is that the model results depend on the value of that parameter. Preliminary experiments with a friction coefficient of 0.3×10^3 m^2 s^{-1} suggest that the variability of large-scale quantities still increases with decreasing friction.

As remarked above, Exp. PE-lo can be considered as the most realistic of all runs and can best be compared with observations. For the interpretation of such a comparison, it would be necessary to assess the internal variability in that model. If the differences in GW position as shown in Table 2 were indicative of the overall dissipation, it would follow that the internal variability in PE-lo were higher than in any of the RG models. From our experiments we have, however, no direct estimate of the internal part of the variability in either of the PE models, due to the prohibitive computational expenses.

In summary, our findings suggest that internal variability is so high that a direct comparison between observations and eddy-resolving models of large-scale quantities like the GW is only meaningful if an ensemble of model experiments is considered. A comparison of actual model realizations to observations would be meaningful only in the context of data assimilation where the

model can be forced to simulate the actual realization of the ocean dynamics.

Friction employed for numerical stability alters the behavior of large-scale quantities, which makes the comparison between data and noneddy-resolving experiments problematic. The meridional location of the GW in the high-friction experiments is significantly different from the low-friction experiments in all the years considered, although the variability in the low-friction experiments is rather high. Observations and experiments with even lower values of friction (not discussed here) indicate that values of about 1° variation for the external and internal variability are at best a lower bound of their real world values. It follows that numerical experiments with higher resolution and/or lower friction values are necessary to model the observed ocean variability of large-scale quantities even at low latitudes as considered here.

Acknowledgements

We thank C. Eden for many helpful remarks and M. Kawamiya for extensive discussions. We are grateful to J.P. McCreary and an anonymous referee for many comments which helped to improve the paper considerably. The altimeter products were produced by the CLS Space Oceanography Division as part of the Environment and Climate EU AGORA (ENV4-CT9560113) and DUACS (ENV44-T96-0357). Support from the German CLIVAR-Ocean project BMBF 03F0246A is gratefully acknowledged. A first version of the PE model used here was set up by N. Rix. We thank the Geophysical Fluid Dynamics Laboratory/NOAA for the prototype code for the OGCM used in the present study, and A. Semtner and R. Chervin for sharing their model data used here at the open boundaries. Figures are prepared using FERRET software.

References

Anderson, D.L.T., Carrington, D.J., 1993. Modeling interannual variability in the Indian Ocean using momentum fluxes from the operational weather analyses of the United Kingdom Meteorological Office and European Centre for Medium Range Weather Forecasts. Journal of Geophysical Research 98, 12 483–12 499.

Barnier, B., Siefridt, L., Marchesiello, P., 1995. Thermal forcing for a global ocean circulation model using a three year climatology of ECMWF analysis. Journal of Marine Systems 6, 363–380.

Bruce, J.G., Fieux, M., Gonella, J., 1981. A note on the continuance of the Somali eddy after the cessation of the Southwest Monsoon. Oceanology Acta 4, 7–9.

Cox, M.D., 1979. A numerical study of Somali current eddies. Journal of Physical Oceanography 9, 311–326.

Evans, R.H., Brown, O.B., 1981. Propagation of thermal fronts in the Somali Current system. Deep-Sea Research I 28A, 521–527.

Fischer, J., Schott, F., Stramma, L., 1996. Currents and transports of the Great Whirl–Socotra Gyre System during the summer monsoon august 1993. Journal of Geophysical Research 101, 3573–3587.

Jensen, T.G., 1993. Equatorial variability and resonance in a wind-driven Indian Ocean Model. Journal of Geophysical Research 98, 22 533–22 552.

Le Traon, P.-Y., Ogor, F., 1998. ERS-1/2 orbit error improvement using Topex/Poseidon: the 2 cm challenge. Journal of Geophysical Research 103, 8045–8057.

Le Traon, P.-Y., Nadal, F., Ducet, N., 1998. An improved mapping method of multi-satellite altimeter data. Journal of Atmospheric and Oceanic Technology 15, 522–534.

Levitus, S., Boyer, T.P., 1994. NOAA Atlas NESDIS 3: World Ocean Atlas 1994, Vol. 3. Technical report, NODC.

Luther, M.E., 1999. Interannual variability in the Somali Current 1954–1976. Non-linear Analyses 35, 59–83.

Luther, M.E., O'Brien, J.J., 1989. Modeling the variability in the Somali Current. In: Nihoul, J.C.J., Jamart, B.M. (Eds.), Mesoscale/Synoptic Coherent Structures in Geophysical Turbulence. Elsevier, Amsterdam, pp. 373–386.

McCreary, J.P., Kundu, P.K., 1989. A numerical investigation of Sea surface temperature variability in the Arabian Sea. Journal of Geophysical Research 94, 16 097–16 114.

McCreary, J.P., Kohler, K.E., Hood, R.R., Olson, D.B., 1996. A four-component ecosystem model of biological activity in the Arabian Sea. Progress in Oceanography 37, 117–165.

Pacanowski, R.C., Philander, S.G.H., 1981. Parameterization of vertical mixing in numerical models of tropical oceans. Journal of Physical Oceanography 11, 1443–1451.

Philander, S.G., 1990. El Niño, La Niña, and the Southern Oscillation. Academic Press, New York, p. 293.

Rix, N., 1998. Variabilität und Wärmetransport in einem numerischen Modell des Indischen Ozeans. Ph.D. Thesis, Institut für Meereskunde Kiel, Germany.

Schott, F., 1983. Monsoon response of the Somali Current and associated upwelling. Progress in Oceanography 12, 357–381.

Schott, F., McCreary Jr., J.P., 2001. The monsoon circulation of the Indian Ocean. Progress in Oceanography 51, 1–123.

Schott, F., Quadfasel, D., 1982. Variability of the Somali Current and associated upwelling. Progress in Oceanography 12, 357–381.

Schott, F., Fischer, J., Garternicht, U., Quadfasel, D., 1997. Winter monsoon circulation of the northern Arabian Sea and Somali Current, 1995. Geophysical Research Letters 24, 2565–2568.

Semtner, A.J., Chervin, R.M., 1992. Ocean general circulation from a global eddy-resolving model. Journal of Geophysical Research 97, 5493–5550.

Stevens, D.P., 1990. On open boundary conditions for three dimensional primitive equation ocean circulation models. Geophysical and Astrophysical Fluid Dynamics 51, 103–133.

Swallow, J.C., Bruce, J.G., 1966. Current measurements off the Somali coast during the southwest monsoon of 1964. Deep-sea Research 13, 861–888.